Energy Storage Materials 14 (2018) 143–148

Contents lists available at ScienceDirect

Energy Storage Materials

journal homepage: www.elsevier.com/locate/ensm

Dendrite-free Li metal anode by lowering deposition interface energy with $Cu_{99}Zn$ alloy coating

Shan Liu[a], Xinyue Zhang[a], Rongsheng Li[b], Libo Gao[b], Jiayan Luo[a,c,*]

[a] Key Laboratory for Green Chemical Technology of Ministry of Education, State Key Laboratory of Chemical Engineering, School of Chemical Engineering and Technology, Tianjin University, Collaborative Innovation Center of Chemical Science and Engineering (Tianjin), Tianjin 300072, China
[b] National Laboratory of Solid State Microstructures, School of Physics, Collaborative Innovation Center of Advanced Microstructures, Nanjing University, Nanjing 210093, China
[c] Key Laboratory of Advanced Energy Materials Chemistry (Ministry of Education), Nankai University, Tianjin, China

ARTICLE INFO

Keywords:
Li metal anodes
Artificial defect
Battery
Interface energy
CuZn alloy

ABSTRACT

Li should be the ultimate anode due to its highest theoretical capacity and lowest electrochemical potentials. However, the dendrite formation has been the grand challenge hindering their direct use. Here we modified the commercial anode Cu current collectors with atomically distributed Zn artificial defects by magnetic sputtering of $Cu_{99}Zn$. Zn has definite solubility in Li metal and can form solid solution before Li metal deposition, lowering the deposition interface energy between current collectors and metal anodes. With atomically distributed seeds, significantly improved performance of Li metal anodes was achieved with depressed dendrite formation on both planar and 3D Cu. The Li-Li symmetric cell can be stably cycled for more than 1000 h. Coulombic efficiency over 98% at Li deposition capacity of 10 mAh cm^{-2} could be maintained. We anticipate that high performance lithium metal batteries could be realized by using this anode combined with optimized electrolytes and cathodes.

1. Introduction

The energy density of lithium (Li) ion batteries is an obstacle that needs to be overcome to fulfill their promise as the energy source for vehicle and electronics. This calls for the use of high energy density materials. Li, having the highest theoretical capacity (3860 mAh g^{-1}) and lowest electrochemical potentials (i.e., −3.04 V vs standard hydrogen electrode), should be the ultimate anode. However, the dendrite formation during deposition associated with Li metal anodes has been the grand challenge hindering their direct use [1,2]. The infinite volume fluctuation of Li electrode and its dendrite formation result in unstable solid electrolyte interphase (SEI) between the Li electrode and electrolyte, limiting the plating/stripping Coulombic efficiency and thus the cycling life of the electrode [3]. The dendrites, if not properly controlled, can lead to hazardous failure when they crossover the separator and electrically short-circuited to the cathodes.

Various strategies [3–10] were proposed aiming to solve the Li dendrite problem during the past few decades, especially when the Li metal anodes are revived in recently years. Electrolyte additives at relative small amount but having the long-lasting dendrite depression effect have been always pursued [5,6,9]. Solid state electrolytes with high ionic conductivity and high interface compatibility with the electrodes have yet been attained [11–13]. Interfacial layers either porous to accommodate the Li dendrites or nonporous to depress the dendrites can be inserted to prevent dendrites penetrating the separator [14–16]. However, the uncontrolled Li nucleation and dendrite growth can become disconnected themselves or weaken the SEI interface during cycling. Hosting Li in a porous scaffold has been proved to be an effective way to suppress dendrite growth [17–28]. The electrode thickness fluctuation is avoided and thus stable SEI is maintained. Such scaffold needs to be conducting, porous, mechanically and chemically stable. As a result, many carbon nanostructures [18,21,24,26–28] and metal foams [17,22,23,25] have been demonstrated effective to support Li.

In all above strategies, the Li deposition substrates have a paramount influence on the plating behaviors. The planar current collectors such as Cu foils and 3D scaffolds such as graphene and Cu foams usually have high interface energy with Li. As a result, Li deposition on these substrates has nucleation overpotential and the nucleation is not uniform. It is found that the Li nuclei size and nuclei number density on Cu depend on the overpotential, which can be tuned to depress dendrite growth [29]. Substrates which have definite solubility in Li

* Corresponding author at: Key Laboratory for Green Chemical Technology of Ministry of Education, State Key Laboratory of Chemical Engineering, School of Chemical Engineering and Technology, Tianjin University, Collaborative Innovation Center of Chemical Science and Engineering (Tianjin), Tianjin 300072, China.
E-mail address: jluo@tju.edu.cn (J. Luo).

https://doi.org/10.1016/j.ensm.2018.03.004
Received 19 February 2018; Received in revised form 5 March 2018; Accepted 5 March 2018
Available online 08 March 2018
2405-8297/ © 2018 Elsevier B.V. All rights reserved.

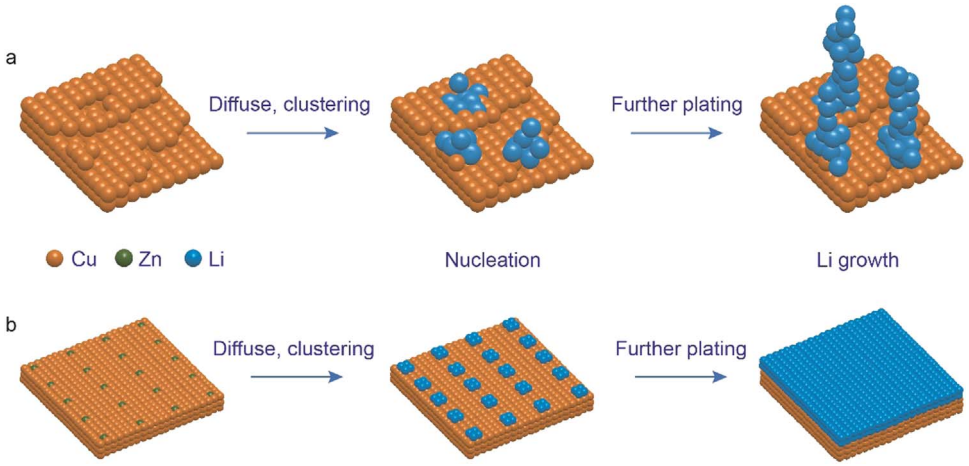


Fig. 1. Schematic showing the Li plating process on the (a) Cu and (b) $Cu_{99}Zn$ substrates.

metal such as Au, Ag, Zn or Mg generate a solid solution buffer layer before Li metal formation, resulting in no overpotential for Li nucleation. These Li soluble materials can be utilized as heterogeneous seeds for Li growth. Indeed, Au nanoparticles in carbon capsules [7], Ag nanoparticles on carbon nanofibers [30], curved carbon granules in Ni foams all improved the Li plating/stripping performance compared to bare scaffolds [20].

For these heterogeneous seeds, controlling their uniformity and coverage is a prerequisite. Here we report the use of atomically distributed seeds with high uniformity and coverage serving as artificial defects to lower the deposition interface energy for stable Li metal anodes. The atomically distributed artificial defects are made by magnetic sputtering of $Cu_{99}Zn$ onto Cu foils or foams (Fig. 1). Several properties of the atomically distributed seeds make them advantageous for lowering the Li deposition interface energy. **1**. Cu foils are commercially used anode current collectors intuitively the compatible substrates for Li metal anodes (Fig. S1) [31]. As a result, porous Cu foams are also widely studied for Li anodes [17,19,22,25]. **2**. Magnetic sputtering can control the atomic ratio and thickness of deposited alloy film with high smoothness, leading to high uniformity and coverage of seeds. **3**. Zn has similar atomic radius to Cu and it can alloy with Cu at almost any atomic ratio without lattice mismatch (Fig. S2) [32]. This ensures the homogeneous distribution of Zn. **4**. Zn has definite solubility in Li metal and can form solid solution before Li metal deposition (Fig. S3) [33], lowering the interface energy. **5**. The facile magnetic sputtering coating is general and can be applicable to modify other planar or 3D substrates. The Zn seeds in deposited films are atomically distributed with coverage tunable simply by adjusting the sputtering targets. Here, we demonstrate that the atomically distributed artificial defects made by magnetic sputtering of $Cu_{99}Zn$ indeed lower the deposition interface energy and significantly improved plating/stripping cycling performance of Li metal anodes on planar and 3D Cu.

2. Experimental section

2.1. Materials

Cu foils (> 99.9%) and 3D Cu (> 99.9%) was purchased from MTI (Hefei). $Cu_{99}Zn$ alloy sputtering target (> 99.9%) was purchased from Zhongnuo Xincai (Beijing) and deposited on to Cu foils and 3D Cu by a customized magnetic sputter (MSP-3200 base pressure < 1E-5 Torr for chamber RF 300 W). The electrolyte salts used was 1 M lithium bis (triflormethanesulfonyl) imide (LiTFSI, 99+%) from Sigma Aldrich. The electrolyte solvents used was 1, 3-dioxolane (DOL, ≥99%) / 1, 2-dimethoxyethane (DME, 99.5%) from Sigma-Aldrich.

2.2. Characterization

SEM (Hitachi S4800, Japan) operated at 5.0 kV was employed to characterize the morphology of Li deposition on Cu and $Cu_{99}Zn$. To transfer the used Li for characterization, after Li was electrodeposited onto Cu and $Cu_{99}Zn$, the cells were opened in the Ar filled glove box and the electrodes were rinsed with fresh 1, 3-dioxolane and dried. Electrodes were mounted onto SEM stages and sealed in Ar-filled transfer vessels for immediate SEM observation. Unavoidable contact with air was brief, and may contribute to some slight surface features on the Li metal seen in SEM images. X-ray powder diffraction (DanDong, China) was employed to characterize the component of sample. The *ex situ* AFM images were scanned directly in argon atmosphere using an AFM apparatus (Bruker, USA) mounted on top of a suspended marble in the glove box.

2.3. Electrochemistry

The Cu and $Cu_{99}Zn$ electrodes were assembled in 2032-type coin cells with Li metal as the reference and counter electrode to evaluate the Columbic efficiency, electrochemical impedance spectra and other properties. The electrolyte was 1 M LiTFSI in DOL/DME. The amount of electrolyte in each cell is 60 µl. To test Columbic efficiency, a fixed amount of Li was deposited on Cu and $Cu_{99}Zn$ anode electrode and then stripped away up to 1.0/1.2 V at various current densities for each cycle. For the symmetrical cell test, 1 mAh cm^{-2} of Li was first plated onto the planar Cu and $Cu_{99}Zn$ at 1.0 mA cm^{-2}, then the cells were cycled at 0.5 mA cm^{-2} for 1 hours in each half cycle. EIS measurements were obtained over the frequency range of 0.1 Hz to 100 KHz with amplitude of 5 mV using a CHI 660 electrochemical workstation. For Li-$LiFePO_4$ full cell, $LiFePO_4$ (MTI, Corp) with an areal capacity of ~ 1 mAh cm^{-2} was used as cathode material. The $LiFePO_4$ electrode was prepared by mixing $LiFePO_4$, Super P, polyvinylidene difluoride (PVDF) in the ratio of 8:1:1 with N-methyl-2-pyrrolidone as the solvent. The 3D Cu and $Cu_{99}Zn$ anodes were deposited with 2 mAh cm^{-2} of Li. For anode free Li-TiS_2 full cell, the 3D Cu and $Cu_{99}Zn$ were directly used as anodes. For TiS_2 electrode, TiS_2, super-P and PVDF were mixed at a weight ratio of 8:1:1 to form homogeneous slurry, and then pasted on Ni foil. The TiS_2 electrodes were pre-lithiated in shorted cells with Li metal and 1 M LiTFSI in DOL/DME electrolyte for 24 h and then dried and paired with 3D Cu and $Cu_{99}Zn$ anodes. After cell assembly, the full cells were galvanostatically charged to 2.6 V prior to cycling.

3. Results and discussion

Fig. 1 illustrates the principle that atomically distributed artificial defects can suppress the Li dendrite growth. On planar or 3D Cu

current collector, inevitably there are defects such as terraces, kinks and steps during their production. The electric field around these defect areas is stronger, which concentrates the Li^+ flux to nucleate. The selective Li nucleation results in uneven Li growth and dendritic and mossy Li forms during plating (Fig. 1**a**). The dendrites can destroy the formed SEI layers which will be patched at the expense of mutually consumption of metal anodes and electrolytes for new SEI formation. Dendrites can also become disconnected easily and pulverize in the long run, losing electric contact. As a result, the notorious dendrite formation is the main contributor for low plating/stripping efficiency of metal anodes and safety hazard if heavily accumulated dendrite short circuits to the cathodes. Instead, with atomically distributed seeds with high coverage and uniformity, the Li nucleation can evolve from these homogenously and atomically distributed artificial defects (Fig. 1**b**). The "un-tendentious" style of nucleation leads to the homogeneous plating of Li metal on the current collectors. Other artificial defect elements can also work with the same principle and this strategy can be extended to other metal anodes.

The $Cu_{99}Zn$ coating was prepared by magnetic sputtering of $Cu_{99}Zn$ alloy onto planar and 3D Cu. With this atomic ratio, there are 4 or 5 Cu atoms in average between two adjacent Zn atoms. The neighboring Zn atom distance is at sub-nanometer scale, ensuring atomically distributed artificial defects. Planar structure is first discussed as it is easier to visualize the effect of artificial defects on suppressing Li dendrite growth. The coating thickness is 70 nm, which can be tuned by the sputtering time (Fig. 2**a**). The coated layer was uniform with high coverage (Fig. S4). Energy dispersive X-ray spectroscopy (EDX) mapping confirmed the homogenously distribution of $Cu_{99}Zn$ in the Cu coating layer (Fig. 2**b**) and the atomic ratio of the coating layer changed slightly from sputtering target through magnetic sputtering process (Fig. S5). Since Zn has similar atomic radius to Cu and it can alloy with Cu at almost any atomic ratio without lattice mismatch (Fig. S2) [32], adding this small amount of Zn didn't alter the crystal structure of Cu (Fig. S6). The appearance of Cu and $Cu_{99}Zn$ coated Cu foils looks the same (Fig. S7). However, they shown obvious differences when used as substrates for Li metal anodes. To visualize the disparity, molten Li was dropped on the two kinds of foils. It is found molten Li remained spherical on the pure Cu foil while spread on $Cu_{99}Zn$ foil with much smaller contact angel (Fig. 2**c inset**). This clearly indicates that the atomically distributed seeds can lower the deposition interface energy. Electrochemically, nucleation overpotential was observed when Li was plated on pure Cu foil (Fig. 2**c**), which is well known for metal anodes. With the atomically distributed seeds, the nucleation overpotential was smoothed at low current densities and much decreased at higher current densities (Fig. 2**c,** Fig. S8), which is consistent with previous reports [29] of direct plating Li on metal substrates with a definite solubility in lithium. As usually observed under scanning electron microscopy (SEM), Li deposited on pure Cu foil was dendritic (Fig. 2**d**). However, the Li plated on $Cu_{99}Zn$ foil was smooth without any protuberance (Fig. 2**e**). The difference in surface topography and roughness of Li deposited on Cu and $Cu_{99}Zn$ foils can be further validated under atomic force microscope (AFM) (Fig. 2**f,g**).

To shed light on how the artificial defect in Cu influences the plating/stripping behavior, the surface morphology of Cu and $Cu_{99}Zn$ foils after different Li plating amount were investigated. From the SEM images of Cu foil with increased Li plating capacity from 0.1 to 1 mAh cm^{-2} using 1 M LiTFSI in DME:DOL (1:1) electrolyte with 1% of $LiNO_3$, Li dendrites were observed initially and become more severe at high loading (Fig. 3**a**). On the contrary, round microparticles were found at low Li loading on $Cu_{99}Zn$ foil. The microparticles got connected and became pancake-like at higher loading and eventually formed a continuous dendrite-free film (Fig. 3**b-d**).

The plating/stripping performance of Li metal anodes on artificial defects coated substrates were tested and compared to that on pure Cu foil. First, 1 mAh cm^{-2} of Li was first deposited onto the Cu and $Cu_{99}Zn$ foils and the symmetric cells were cycled at constant current of 0.5 mA cm^{-2} in ether electrolyte with plating/stripping capacity of 0.5 mAh cm^{-2} (Fig. 3**e**). The voltage hysteresis of the cell using planar Cu foil electrode gradually increased and the cell was shorted after 500 h (250 cycles). While in the cell with $Cu_{99}Zn$ electrode, the voltage

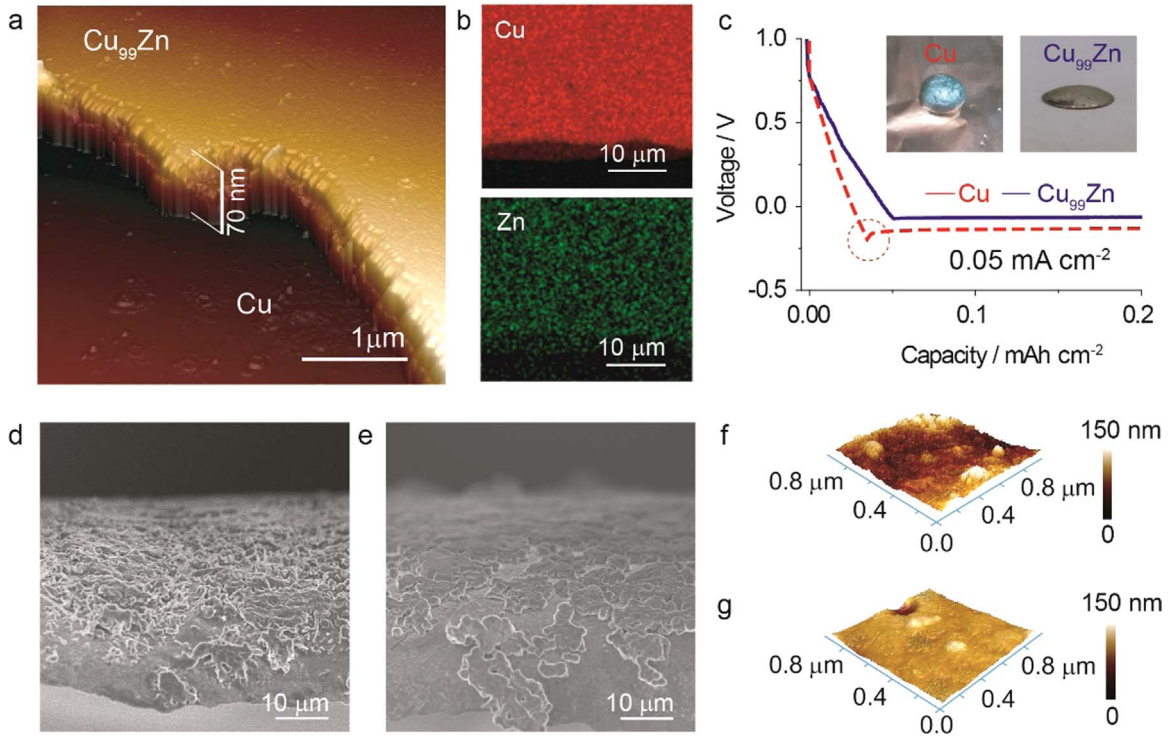


Fig. 2. Dendrite-free Li plating on $Cu_{99}Zn$. (a) AFM image and (b) EDX mapping of $Cu_{99}Zn$ sputtered on Cu foil. (c) Voltage profiles during initial Li plating at 0.05 mA cm^{-2} on the Cu and $Cu_{99}Zn$. The inset shows the wetting behavior of molten Li on Cu and $Cu_{99}Zn$. Cross-section SEM images of (d) Cu and (e) $Cu_{99}Zn$ after plating 0.2 mAh cm^{-2} Li. AFM images of (f) Cu and (g) $Cu_{99}Zn$ with plated 0.1 mAh cm^{-2} of Li.

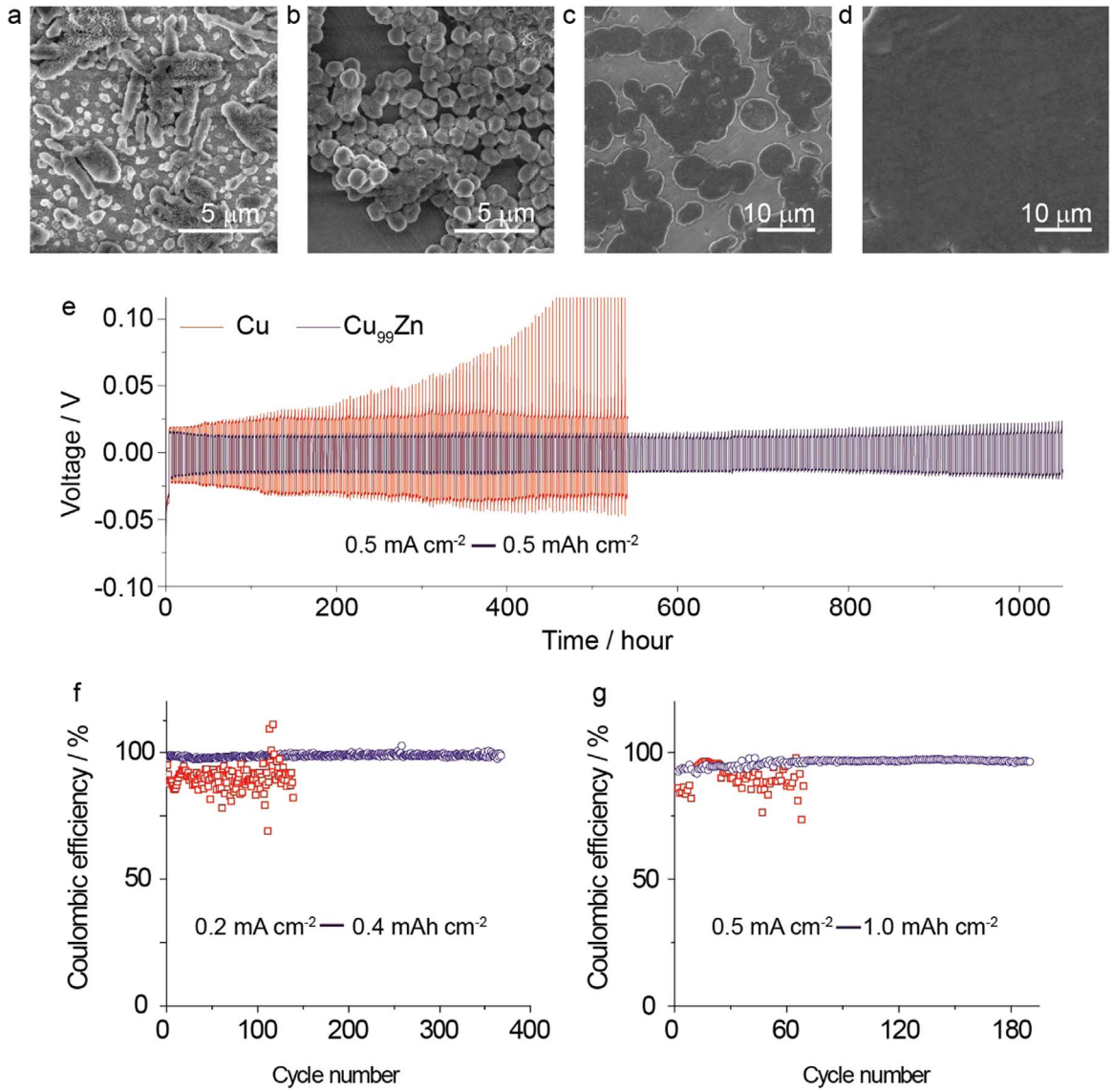


Fig. 3. Morphology and electrochemical performance of Li plating on planar Cu and $Cu_{99}Zn$. (a) SEM image of 0.1 mAh cm^{-2} of Li plated on Cu. SEM images of (b) 0.1 mAh cm^{-2}, (c) 0.5 mAh cm^{-2}, (d) 1.0 mAh cm^{-2} of Li plated on $Cu_{99}Zn$ at current density of 1.0 mA cm^{-2}. (e) Voltage profiles of Li plating/stripping in symmetrical cells. 1 mAh cm^{-2} of Li was first deposited on substrates. Coulombic efficiency of Li plating/stripping on planar Cu and $Cu_{99}Zn$ (f) with plating capacity of 0.4 mAh cm^{-2} at current density of 0.2 mA cm^{-2} and (g) with plating capacity of 1 mAh cm^{-2} at current density of 0.5 mA cm^{-2}.

hysteresis was smaller and maintained unchanged for more than 1000 h (500 cycles), indicating improved plating/stripping stability of artificial defects. The $Cu_{99}Zn$ coating layer was stable during Li plating/stripping. EDX elemental mapping images of $Cu_{99}Zn$ alloy coating after 100 cycles indicated cycling confirmed Zn was homogenously distributed in the coating layer after cycling (Fig. S9). The Coulombic efficiency of $Cu_{99}Zn$ foils was first studied in half-cell configuration with Li metal as the counter electrode and Li source, in comparison to pure Cu foils. Li was first plated onto the Cu and $Cu_{99}Zn$ foils at a fixed amount and then stripped away to 1 V (Fig. 3**f,g**). Their average Coulombic efficiency of $Cu_{99}Zn$ foils was 99% over 400 cycles at current density of 0.2 mA cm^{-2} and 97% over 200 cycles at current density of 0.5 mA cm^{-2}, respectively, which are significantly higher than bare Cu electrodes (drop to below 79% after 300 cycles and 73% after 70 cycles, respectively). More importantly, the Coulombic efficiency of $Cu_{99}Zn$ electrodes was relatively stable while there was much larger fluctuation for bare Cu electrodes. The lower Coulombic efficiency of bare Cu electrodes reflects the unstable SEI. And the large fluctuation can be attributed to the fracture of Li filament and dendrite, and the occasional reconnection of the fractured pieces from previous cycles.

3D substrates typically outperform planar ones for Li metal anodes because their geometric surface area are higher than planar ones, which can largely increase the available surface for Li to nucleate. At the same time, the effective current density for plating/stripping on substrates will be lowered, and thus the Li growth rate. Moreover, the SEI layers on 3D substrates are more stable than on planar ones as 3D substrates can accommodate some amount of Li deposited inside without destroying the top SEI layers but the thickness fluctuation of Li plating on planar substrates is infinite. $Cu_{99}Zn$ coating was performed on 3D Cu by magnetic sputtering (Fig. S10). As observed in Fig. 4**a,b**, the pores in the 3D Cu were at tens of micrometer scale and the $Cu_{99}Zn$ was conformably coated. With increased Li plating amounts from 0.5 to 2 mAh cm^{-2}, Li grown first in the 3D $Cu_{99}Zn$ skeleton and gradually filled the pores without any obvious dendrites (Fig. 4**c-e**). If the thickness of the 3D $Cu_{99}Zn$ electrodes increases (~100 μm in this work), the Li deposit amount within the 3D $Cu_{99}Zn$ can be can improved. Even larger amount of Li deposits would be plated on top of the scaffolds after the pores are filled with dendrite-free smooth surface (Fig. S11). However, dendrites on 3D Cu were observed at the same loading (Fig. S12). At high plating/stripping capacity and/or higher current density, the 3D $Cu_{99}Zn$ all

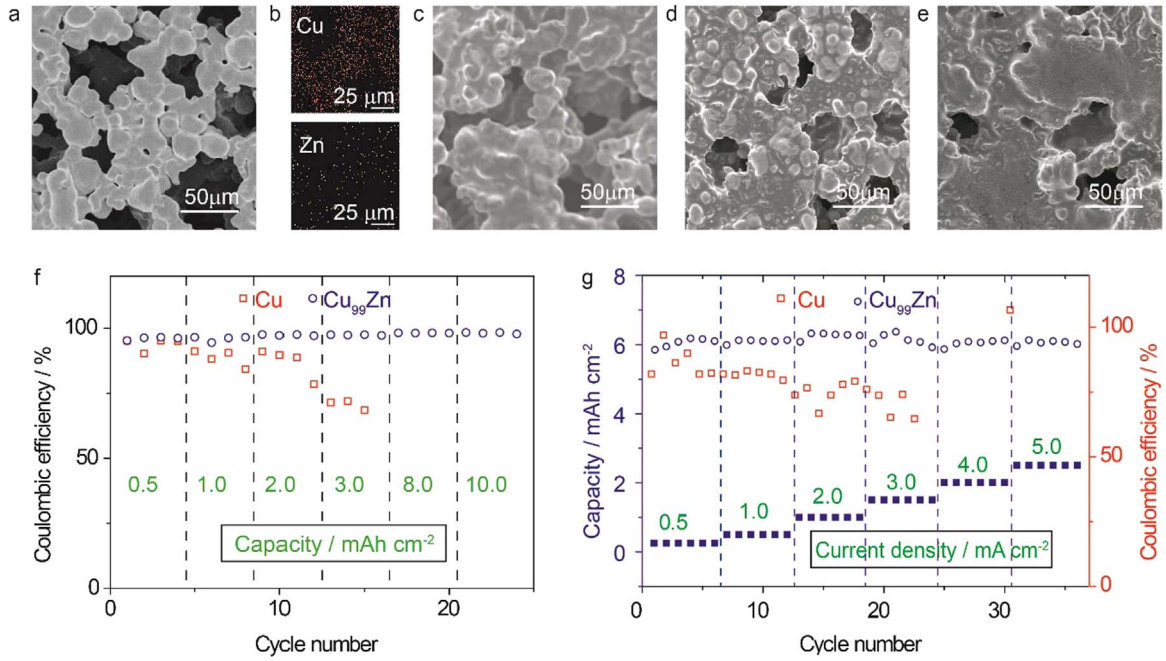


Fig. 4. Morphology and electrochemical performance of Li plating on 3D Cu and $Cu_{99}Zn$. (a) SEM image of 3D Cu coated with $Cu_{99}Zn$ and (b) the corresponding EDX mapping. SEM images of 3D $Cu_{99}Zn$ after plating (c) 0.5 mAh cm^{-2}, (d) 1.0 mAh cm^{-2}, (e) 2.0 mAh cm^{-2} of Li. (f) Coulombic efficiency of Li plating/stripping on the 3D Cu and $Cu_{99}Zn$ with increased capacity at current density of 1.0 mA cm^{-2}. (g) Coulombic efficiency of Li plating/stripping on the 3D Cu and $Cu_{99}Zn$ with increasing current density. Each plating/stripping cycle was 1 h.

outperform 3D Cu electrodes. The 3D $Cu_{99}Zn$ could maintain Coulombic efficiency over 98% at Li deposition capacity of 10 mAh cm^{-2} and over 94% at current density of 5 mA cm^{-2}, while the bare Cu electrode dropped to below 71% at capacity of 4 mAh cm^{-2} or below 73% at current density of 3 mA cm^{-2} (Fig. 4**f,g and** Fig. S13). The 3D $Cu_{99}Zn$ also had better performance than 3D Cu electrode in ester based electrolyte. With 1 M $LiPF_6$ in EC/DEC electrolyte, the Coulombic efficiency of pure 3D Cu started to decay after 70 cycles while the $Cu_{99}Zn$ coated Cu could maintain stable for 200 cycles at Li deposition capacity of 0.5 mAh cm^{-2} at current density of 0.5 mA cm^{-2} (Fig. S14). Electrochemical impedance of the 3D $Cu_{99}Zn$ and 3D Cu electrodes during Li plating/stripping illustrated that the 3D $Cu_{99}Zn$ had much lower charge transfer resistance in the first cycle and remained stable after cycling (Fig. S15). However, the 3D Cu had larger initial resistance and kept increasing after cycling due to its low Coulombic efficiency and unstable SEI. The 3D Cu and $Cu_{99}Zn$ electrodes were assembled into anode-free Li-TiS_2 full cells with pre-lithiated TiS_2 cathodes (Fig. S16**a**). The cell with 3D $Cu_{99}Zn$ electrode shown much better cycling stability compared to that with pure Cu (Fig. S16**b**). Full cells with $LiFePO_4$ cathodes were also assembled. The 3D Cu and $Cu_{99}Zn$ electrodes were deposited with 2 mAh cm^{-2} Li as the anodes before full cell assembly. The $Cu_{99}Zn$ cell could maintain stable over 100 cycles but the cell with pure Cu shown fast fading after 40 cycles (Fig. S17).

4. Conclusion

In summary, we propose that the atomically distributed artificial defects of Zn in $Cu_{99}Zn$ can lower the deposition interface energy between Cu current collectors and Li metal anodes and significantly improve the plating/stripping cycling performance of Li metal anodes on planar and 3D Cu. With atomically distributed seeds with high coverage and uniformity, the Li nucleation can evolve from these homogenously and atomically distributed artificial defects, leads to the homogeneous plating of Li metal on the current collectors. The Li-Li symmetric cell with planar $Cu_{99}Zn$ electrode can be cycled for more than 1000 h with small and stable voltage hysteresis. The 3D $Cu_{99}Zn$ electrode could maintain Coulombic efficiency over 98% at Li deposition capacity of 10 mAh cm^{-2}. Optimizing the chemical composition and content of artificial defects could definitely further improve the electrochemical performance, which is under investigation. This scalable surface coating strategy is compatible with commercial anode current collectors and paves the way for Li metal anodes.

Acknowledgements

The authors appreciate support from National Natural Science Foundation of China (Grant Nos. 51502197, U1601206), Natural Science Foundation of Tianjin, China (Grant Nos. 17JCJQJC44100, 15JCYBJC53100), Thousand Youth Talent Plan and Tianjin University.

Appendix A. Supporting information

Supplementary data associated with this article can be found in the online version at doi:10.1016/j.ensm.2018.03.004.

References

[1] J.M. Tarascon, M. Armand, Nature 414 (2001) 359–367.
[2] M. Armand, J.M. Tarascon, Nature 451 (2008) 652–657.
[3] N. Liu, Z. Lu, J. Zhao, M.T. McDowell, H.W. Lee, W. Zhao, Y. Cui, Nat. Nano 9 (2014) 187–192.
[4] K. Yan, H.W. Lee, T. Gao, G. Zheng, H. Yao, H. Wang, Z. Lu, Y. Zhou, Z. Liang, Z. Liu, Y. Cui, Nano Lett. 14 (2014) 6016–6022.
[5] F. Ding, W. Xu, G.L. Graff, J. Zhang, M.L. Sushko, X. Chen, Y. Shao, M.H. Engelhard, Z. Nie, J. Xiao, J. Am. Chem. Soc. 135 (2013) 4450–4456.
[6] Y. Lu, Z. Tu, L.A. Archer, Nat. Mater. 13 (2014) 961–969.
[7] R. Mukherjee, A.V. Thomas, D. Datta, E. Singh, J. Li, O. Eksik, V.B. Shenoy, N. Koratkar, Nat. Commun. 5 (2014) 3710–3720.
[8] Y. Liu, D. Lin, Z. Liang, J. Zhao, K. Yan, Y. Cui, Nat. Commun. 7 (2016) 10992.
[9] W. Li, H. Yao, K. Yan, G. Zheng, Z. Liang, Y.M. Chiang, Y. Cui, Nat. Commun. 6 (2015) 7436.
[10] J. Qian, W.A. Henderson, W. Xu, P. Bhattacharya, M. Engelhard, O. Borodin, J.G. Zhang, Nat. Commun. 6 (2015) 6362.
[11] Z. Tu, P. Nath, Y. Lu, M.D. Tikekar, L.A. Archer, Acc. Chem. Res. 48 (2015) 2947–2956.
[12] X. Han, Y. Gong, K. Fu, X. He, G.T. Hitz, J. Dai, A. Pearse, B. Liu, H. Wang, G. Rubloff, Y. Mo, V. Thangadurai, E.D. Wachsman, L. Hu, Nat. Mater. 16 (2017) 572–579.
[13] K. Fu, Y. Gong, B. Liu, Y. Zhu, S. Xu, Y. Yao, W. Luo, C. Wang, S.D. Lacey, J. Dai, Y. Chen, Y. Mo, E. Wachsman, L. Hu, Sci. Adv. 3 (2017) e1601659.
[14] X.B. Cheng, T.Z. Hou, R. Zhang, H.J. Peng, C.Z. Zhao, J.Q. Huang, Q. Zhang, Adv. Mater. 28 (2016) 2888–2895.

[15] Y. Liu, D. Lin, P.Y. Yuen, K. Liu, J. Xie, R.H. Dauskardt, Y. Cui, Adv. Mater. 29 (2017) 1605531.
[16] B. Zhu, Y. Jin, X. Hu, Q. Zheng, S. Zhang, Q. Wang, J. Zhu, Adv. Mater. 29 (2017) 1603755.
[17] C.P. Yang, Y.X. Yin, S.F. Zhang, N.W. Li, Y.G. Guo, Nat. Commun. 6 (2015) 8058.
[18] D. Lin, Y. Liu, Z. Liang, H.W. Lee, J. Sun, H. Wang, K. Yan, J. Xie, Y. Cui, Nat. Nano. 11 (2016) 626.
[19] L.L. Lu, J.J. Ge, N. Yang, S.M. Chen, H. Yao, F. Zhou, S.H. Yu, Nano Lett. 16 (2016) 4431–4437.
[20] H. Ye, S. Xin, Y.X. Yin, J.Y. Li, Y.G. Guo, L.J. Wan, J. Am. Chem. Soc. 139 (2017) 5916–5922.
[21] T.T. Zuo, X.W. Wu, C.P. Yang, Y.X. Yin, H. Ye, N.W. Li, Y.G. Guo, Adv. Mater. 29 (2017) 1700389.
[22] Q. Yun, Y.B. He, W. Lv, Y. Zhao, B. Li, F. Kang, Q.H. Yang, Adv. Mater. 28 (2016) 6932–6939.
[23] Y. Li, J. Jiao, J. Bi, X. Wang, Z. Wang, L. Chen, Nano Energy 32 (2017) 241–246.
[24] G.S. Zheng, W. Lee, Z. Liang, H.W. Lee, K. Yan, H. Yao, H. Wang, W. Li, S. Chu, Y. Cui, Nat. Nano. 9 (2014) 618–623.
[25] Q. Li, S. Zhu, Y. Lu, Adv. Funct. Mater. (2017) 1606422.
[26] R. Zhang, X.B. Cheng, C.Z. Zhao, H.J. Peng, J.L. Shi, J.Q. Huang, J. Wang, F. Wei, Q. Zhang, Adv. Mater. 28 (2016) 2155–2162.
[27] Z. Liang, D. Lin, J. Zhao, Z. Lu, Y. Liu, C. Liu, Y. Lu, H. Wang, K. Yan, X. Tao, Y. Cui, Proc. Natl. Acad. Sci. 113 (2016) 2862–2867.
[28] S. Jin, Z. Sun, Y. Guo, Z. Qi, C. Guo, X. Kong, Y. Zhu, H. Ji, Adv. Mater. (2017) 1700783.
[29] K. Yan, Z. Lu, H.W. Lee, F. Xiong, P.C. Hsu, Y. Li, J. Zhao, S. Chu, Y. Cui, Nat. Energy 1 (2016) 16010.
[30] C. Yang, Y. Yao, S. He, H. Xie, E. Hitz, L. Hu, Adv. Mater. (2017) 1702714.
[31] A. Pelton, J. Phase Equilib. 7 (1986) 142–144.
[32] R. Ruer, K. Kremers, Z. Anorg. Chem. 184 (1929) 193–231.
[33] A. Pelton, J. Phase Equilib. 12 (1991) 42–45.